applied sciences

MDPI

Article

Deposition of CAP/Antioxidants Systems on Silica Particles Using the Supercritical Antisolvent Process

Ignacio García-Casas, Antonio Montes *, Diego Valor, Clara Pereyra and Enrique J. Martínez de la Ossa

Department of Chemical Engineering and Food Technology, Faculty of Sciences, University of Cádiz, International Excellence Agrifood Campus (CeiA3), 11510 Puerto Real (Cádiz), Spain; ignacio.casas@uca.es (I.G.-C.); diego.valor@uca.es (D.V.); clara.pereyra@uca.es (C.P.); enrique.martinezdelaossa@uca.es (E.J.M.d.l.O.)

* Correspondence: antonio.montes@uca.es

Received: 9 June 2020; Accepted: 26 June 2020; Published: 1 July 2020

Abstract: Supercritical carbon dioxide has been used to deposit co-precipitates of natural antioxidants with a polymer onto silica microparticles. The supercritical antisolvent process (SAS) was carried out with the antioxidants by introducing the silica microparticles into the precipitator vessel. Two different configurations were employed to pump the solution. In one configuration, the antioxidant and the polymer were dissolved and injected together through a nozzle. In the second configuration, the antioxidant and the polymer were dissolved in different solutions and sprayed through different nozzles. The use of operating conditions significantly above the critical point (180 bar and 323 K) led to the formation of composites made up of co-precipitates and silica. Delivery profiles showed that the presence of the polymer and the silica delayed release of the antioxidant into gastric media, thus protecting it and allowing its full delivery to the intestinal fluids to improve the effectiveness of the antioxidant.

Keywords: supercritical deposition; quercetin; mangiferin; cellulose acetate phthalate; supercritical antisolvent process

1. Introduction

The development of new scientific techniques to improve aspects of life in an environmentally friendly way is demanded by society in general and is a principle that is addressed by the scientific community. In recent years, the use of CO_2 under supercritical conditions (i.e., above 304.1 K and 73.8 bar) has been considered as a green and environmentally friendly evolution when compared to more conventional methods [1,2]. The effectiveness of this approach in processes involving extraction [3,4], micronization [5,6], encapsulation [7,8] or impregnation [9,10], while removing or reducing the use of organic solvents that were widely used decades ago in industry, represents a great advance in meeting the current demands of society.

In accordance with the above principles, the supercritical antisolvent process (SAS) exploits the ability to precipitate compounds that are not soluble in supercritical CO_2. A solution of an active substance is sprayed through a nozzle into a precipitator that contains CO_2 under supercritical conditions. Once the substances are in contact, $scCO_2$ diffuses into the organic solvent, thus leading to supersaturation of the solution, which in turn results in precipitation of the active substance. A large number of authors have used this method [11,12] to micronize or encapsulate various substances.

In the work described here, the matrix selected to deposit the antioxidants as precipitates was mesoporous SB-300 silica, mainly due to its large specific surface area and high porosity [13]. Some authors have already studied supercritical impregnation onto porous matrixes such as activated

carbon, carbon-sulfur composites [14], silica MCM-41 with nanometallic (Ru, Rh, Pd) and bimetallic (Ru-Rh, Ru-Pd, Rh-Pd) deposition [15] or cobalt oxide nanoparticles [16] on MCM-41, Pd nanoparticles into mesoporous silica SBA-15 [17], or Ru nanoparticles onto SiO_2 SBA-15 [18]. In the study described here, the aim was to examine the supercritical deposition of a natural antioxidant and to carry out an in-depth study into the effects of different SAS configurations.

The active principles selected were quercetin (Q), a flavonoid with a range of relevant properties such as anti-inflammatory, antibacterial, anticancer and cardiovascular health [19,20], and mangiferin (MNG), a common polyphenol with numerous therapeutic treatments that include anti-viral, anti-oxidant or anti-diabetic activities [21,22]. The effect of these active principles is very small due to their low solubility in water, which complicates oral delivery and bioavailability [23,24]. The use of an SAS process reduces the particle size of these compounds and enhances the solubility in aqueous media. The micronization of MNG and Q using a SAS process has previously been studied by several authors. Micro- (MPs) and nanoparticles (NPs) of MNG were obtained by Liu et al. [25] using N,N-dimethylformamide (DMF) as co-solvent to give MPs with an average size of 0.53 μm. Montes et al. [26] obtained MPs and NPs with sizes between 0.22 and 1.44 μm using acetone and dimethyl sulfoxide (DMSO) as a co-solvent. As far as Q is concerned, MPs and NPs were obtained by several authors [27]. For example, Santos et al. reduced the particle size by a factor of 4.1 [28], Kakran et al. obtained MPs and NPs with sizes between 0.12 and 0.45 μm, Fernandez-Ponce et al. [29] succeeded in precipitating MPs and NPs with sizes between 0.15 and 0.35 μm and Montes et al. [30] successfully precipitated MPs and NPs with sizes between 0.15 and 1.25 μm.

The coating agent selected was cellulose acetate phthalate (CAP), a cellulose derivative that has previously been studied [31] and used to control drug delivery [32] due to its resistance to gastric fluids and its degradation in intestinal fluids at a pH of around 6.8 [33].

In the study reported here, co-precipitates of CAP/Q and CAP/MNG were precipitated on silica particles by an SAS process using one (SAS1) or two (SAS2) nozzles. The typical conditions for the SAS process were selected by considering previous co-precipitation studies on CAP/Q and CAP/MNG [31,34]. The aim of this study was to test the feasibility of forming compounds composed of co-precipitates with a porous matrix located inside the precipitator. The release and dissolution profiles of the quercetin and mangiferin composites were also studied.

2. Materials and Methods

2.1. Materials

Quercetin ($C_{15}H_{10}O_7$), cellulose acetate phthalate ($C_{116}H_{116}O_{64}$), acetone (99.5%), ethanol (99.5%), and dimethyl sulfoxide (DMSO) (99.9%) were obtained from Sigma-Aldrich, Madrid, Spain and mangiferin ($C_{19}H_{18}O_{11}$) was purchased from Glentham Life Science, Corsham, U.K. Spheres of mesoporous SB-300 silica were provided by Miyoshi Europe Laboratories S.A., Lyon, France. CO_2 with a minimum purity of 99.8% was supplied by Linde, Puerto Real, Spain.

2.2. SAS Process

The SAS process was used to carry out the precipitation of the antioxidant and polymer onto silica particles. This process was carried out on the SAS200 system developed by Thar Technologies®. This equipment consists of a CO_2 bottle, two high pressure pumps to pump the CO_2 into the system and the organic solution into the precipitation chamber, a thermostatic bath to cool the CO_2 so that it can be pumped by the high-pressure pump, a 0.5 L stainless steel pressure vessel, a pressure regulator to control the pressure in the precipitation chambers, and a 0.5 L stainless steel separator to separate the solvent and the CO_2, thus avoiding the expulsion of organic solvent to the outside. The equipment also has auxiliary elements, such as heat exchangers—a low-pressure one that is used to cool the CO_2 before it enters the pump and a second heat exchanger (high pressure), electric in this case, that preheats the CO_2 at the entrance of the precipitation vessel to reach the desired conditions more

rapidly. The plant also has pressure devices (manometers), which are located in the pumps, the precipitation vessel, and the separator. The temperature is controlled by thermocouples located inside and outside the precipitation vessel and in the separator. Finally, the flow is controlled by a mass flow meter (FlexCORTM), which measures the flow at the entrance of the system. Pressure, temperature, and flow are controlled by the Process Suite software developed by Thar Technologies.

In all tests, a polymer/antioxidant ratio of 2:1 was chosen on the basis of previous work in which the feasibility of co-precipitating these compounds with ratios of 1:1 to 1:10 was confirmed. In the SAS1 process, the ratio did not affect the particle size of the precipitates but in the SAS2 this parameter could be affected because the concentrations of the injected solutions are changed in order to maintain the same concentration in each solution [34]. An injection flow rate of 6 mL/min for the solutions, a nozzle diameter of 100 µm, and a drying time of 90 min were used. Fixed operating conditions, such as pressure, temperature, and flow variables, were established in previous co-precipitation studies [31,34] (Table 1). Initially, a fixed amount of silica, 500 mg, was deposited into the precipitator and once the operating conditions were reached, the co-precipitates were injected using the SAS1 or SAS2 configuration. The P and T conditions were overestimated in order to ensure that the conditions were above the DMSO/acetone/CO_2 [35,36] and ethanol/CO_2 mixture critical points [37] due to the presence of the silica inside the precipitation vessel. The presence of silica could influence the phase equilibrium. The two configurations employed in the SAS process are described in Sections 2.2.1 and 2.2.2.

Table 1. Summary of supercritical antisolvent process (SAS) experiments carried out.

Exp.	Pressure (bar)	Temperature (K)	CO_2 Flow Rate (g/min)	Process	Co-Precipitate
1	90	313	30	SAS2	CAP/Q
2	90	313	10	SAS2	CAP/Q
3	90	313	30	SAS1	CAP/Q
4	90	313	10	SAS1	CAP/Q
5	180	323	30	SAS2	CAP/MNG
6	180	323	30	SAS1	CAP/MNG
7	180	323	30	SAS1	CAP/Q
8	180	323	30	SAS2	CAP/Q

Supercritical antisolvent process using one (SAS1) or two (SAS2) nozzles; CAP (cellulose acetate phthalate); Q (quercetin); MNG (mangiferin).

2.2.1. Supercritical Antisolvent Process Using One Nozzle (SAS1)

In this process, quercetin or mangiferin and CAP were dissolved together in 50 mL of a 2:1 mixture of ethanol or acetone/DMSO, respectively, with a concentration of 20 mg/mL. The mixtures were stirred magnetically for 30 min. CO_2 was blown into a precipitator vessel to reach the pressure and temperature required. The liquid mixture was then injected into the vessel and sprayed through a nozzle with a diameter of 100 µm. The $scCO_2$ rapidly dissolved in the organic solution during the mixture and this led to the precipitation of the solutes due to the anti-solvent effect (Figure 1).

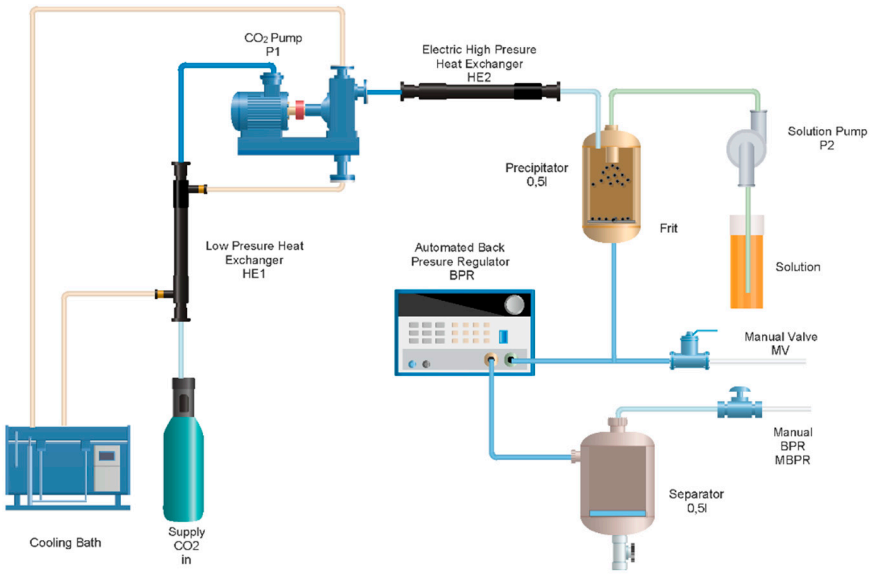

Figure 1. Schematic diagram of the supercritical antisolvent device, SAS1.

2.2.2. Supercritical Antisolvent Process Using Two Nozzles (SAS2)

In this configuration (Figure 2), CAP and the antioxidant (Q and MNG) were dissolved as separate solutions in ethanol for CAP and Q, and in acetone/DMSO for CAP and MNG experiments. These solutions were pumped into the precipitator vessel through two different nozzles, each 100 µm in diameter. In this case, each 50 mL of solution had a concentration of 20 mg/mL (Q or MNG) and 40 mg/mL (CAP) in order to maintain a 1:2 ratio and the dissolution flow rate was the same for both solutions.

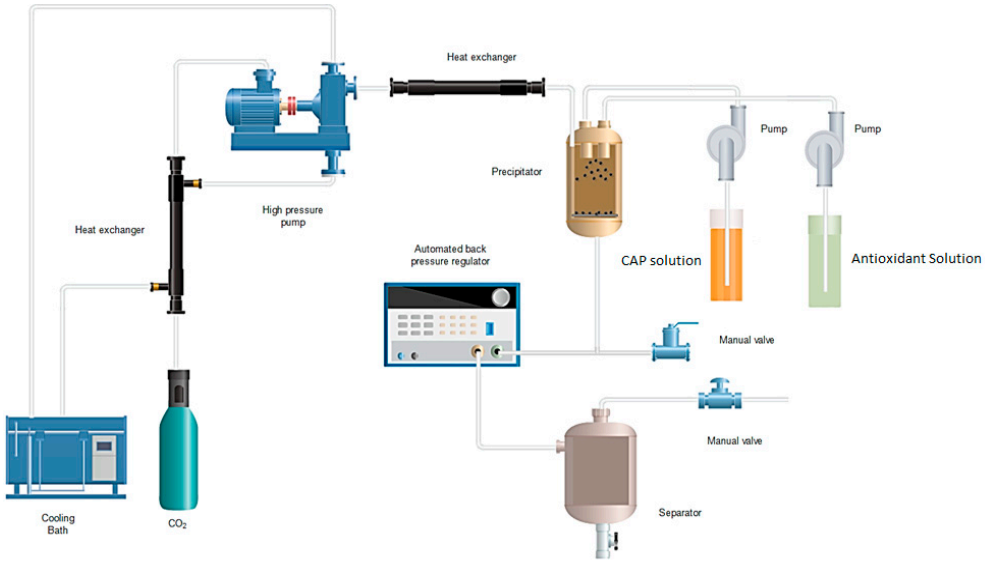

Figure 2. Schematic diagram of the supercritical antisolvent device, SAS2.

2.3. Scanning Electron Microscopy

The morphologies of the samples were analyzed with a Nova NanoSEM 450 field-emission scanning electron microscope (SEM) with 1 nm ultimate resolution. High-vacuum operations were carried out during sample analyses. It is possible to observe secondary and backscattered electrons under various conditions thanks to several detectors and to obtain STEM images. The images were

taken from powder samples placed on a carbon tape and coated with a 15 nm film of gold under an argon atmosphere prior to analysis.

2.4. Release Tests

Solutions of intestinal fluid (SIF) and simulated gastric fluid (SGF) were prepared as follows. In order to make SIF, a solution of 6.8 g/L of monobasic potassium phosphate in distilled water was prepared and adjusted to pH 6.8 ± 0.1 with 0.2 M NaOH. SGF was prepared by dissolving 2 g of sodium chloride in 1 L of distilled water and adjusting the pH to 1.2 ± 0.1 with 0.2 N HCl.

Samples of co-precipitates (5 mg) were added to 40 mL of simulated fluid in each release experiment. The experiments were carried out at 37 °C and 165 rpm. Aliquots (3 mL) of each sample were removed for measurement at certain intervals of time up to 8 h. Prior to analysis, the samples were filtered through a Teflon filter (0.45 μm). Each sample was replaced by an equal amount of fluid. A Shimadzu UV-VIS mini spectrophotometer with λ 365 nm was used to measure the quantity of quercetin and mangiferin present in these aliquots. Calculation of the corrected concentration of released quercetin and mangiferin was carried out as defined by Zhu et al. [38].

3. Results and Discussion

3.1. SAS1 and SAS2 Experiments

This study was focused on the variation of the CO_2 flow rate and how the two configurations (SAS1 and SAS2) affected the deposition (see Supplementary Materials). The results of experiments 1–4, in which the co-precipitates are CAP/Q, are provided in Table 1. In these experiments a pressure of 90 bar, a temperature of 313 K, and a constant dissolution rate of 6 mL/min were fixed for all experiments, the CO_2 flow rate varied from 10 to 30 g/min, and the appropriate SAS process configuration. The results measured at the bottom of the precipitation vessel in the experiments are provided in Figure 3. It can be observed that in experiments 1, 3, and 4 there was precipitation on the bottom of the vessel, on the wall, and on the nozzle. However, in experiment 2 there was only precipitation on the wall of the vessel. It is important to note that the silica particles were located on the bottom of the vessel. In these experiments, the bottom of the vessel appeared wet with residual organic solvent. This observation could be due to the fact that the experiments were carried out very close to the MCP, which for DMSO/acetone/CO_2 are 79.7 bar at 313 K and 89.6 bar at 323 K, [35,36] and for ethanol/CO_2 are 79.4 bar at 313.4 K and 89.8 bar at 322.5 K [37]. This situation would cause a subcritical process that cannot remove all of the organic co-solvent. In the experiments carried out with a higher flow rate of CO_2 (exp. 1 and 3), the bottom of the vessel was covered with a large quantity of particles—more than in exp. 2 and 4. This could be caused by an increase in the turbulence near to the jet generating a higher supersaturation [39] and providing a higher efficiency in the micronization. The SEM images for experiments 1–4 (Figure 4) did not show the presence of silica particles, which are spherical particles of around 3–8 μm (as provided by the manufacturer, the Miyoshi laboratory) [13]. The spherical particles correspond to the precipitation of CAP and the rectangular sticks were identified as precipitated Q.

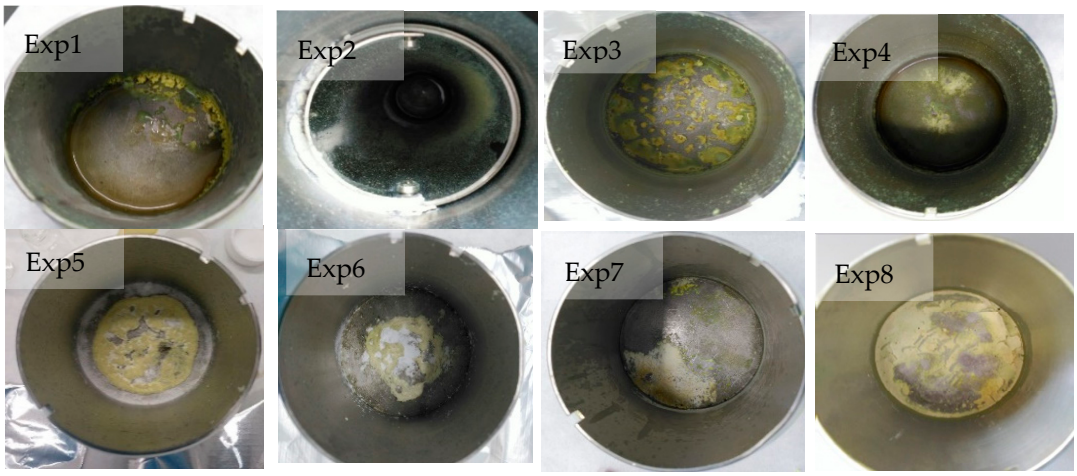

Figure 3. Deposition images of the bottom of the precipitator vessel, experiments 1–8.

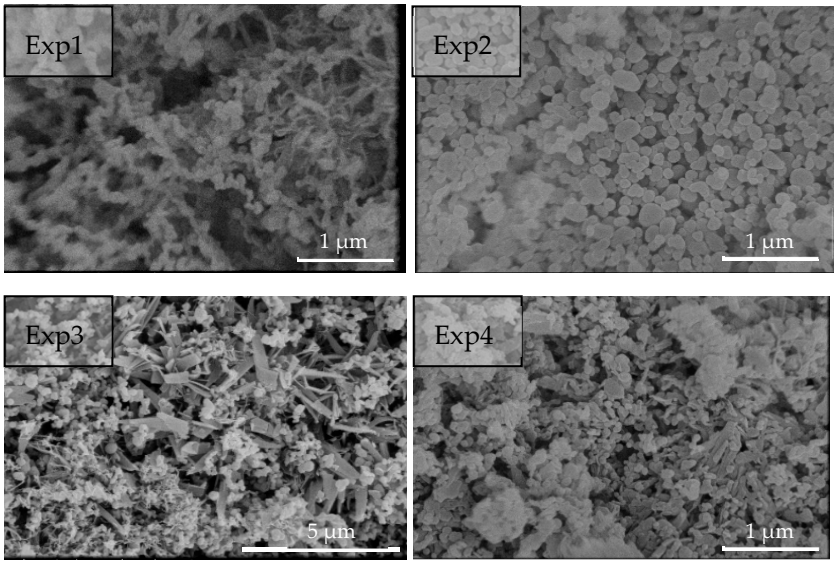

Figure 4. SEM images for deposition experiments 1–4.

The images of the precipitates on the bottom of the vessel in deposition experiments 5 and 6 are shown in Figure 3 and these correspond to CAP/MNG co-precipitates. It can be observed that almost all compounds were deposited on the bottom of the vessel to form a "body-mass". The SEM images of these "body-mass" solids (Figure 5) for both configurations showed the presence of silica particles and CAP/MNG co-precipitates. In this case, a slight variation in the morphologies of the particles between SAS1 and SAS2, as observed in a previous study [34], was found. SAS2 co-precipitate particles (exp. 5) showed two different morphologies (quasi-spherical and sticks) against one morphology (quasi-spherical) for the particles observed for co-precipitates with SAS1. It is remarkable that the micronization of MNG also led to quasi-spherical particles and the raw MNG particles are sticks [26]. It can be argued that with the double injection the amorphization of the MNG did not occur and particles similar to the raw material, i.e., with some degree of crystallinity, were formed.

In these experiments one could observe the difference between the silica particles, which are spherical particles of 3–8 µm, and the spherical particles and sticks corresponding to co-precipitated CAP/MNG, which were smaller.

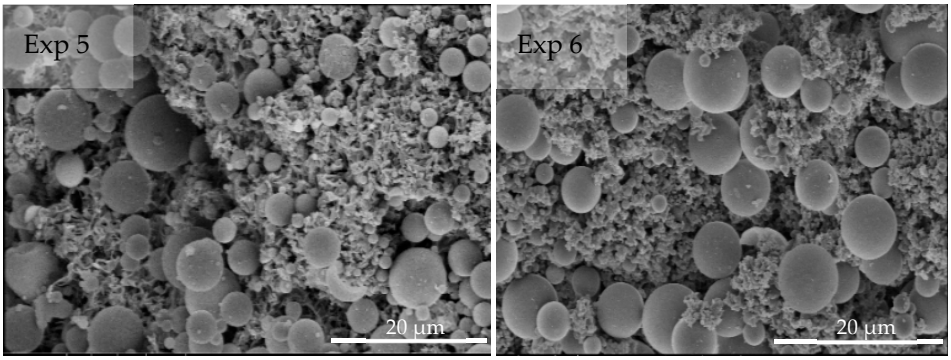

Figure 5. SEM images for deposition experiments 5 and 6.

Finally, experiments 7 and 8 were carried on the CAP/Q co-precipitates under the same conditions as experiments 5 and 6 due to the successful results obtained with these conditions. In this case, the increase in the pressure from 90–180 bar avoided the possible complications related to being in subcritical conditions and the CO_2 flow rate was fixed at 30 g/min. The bottom of the vessel was free of co-solvent for both configurations of the SAS process (see Figure 3) and a similar dry "body-mass" as in experiments 5 and 6 was observed. The SEM images (Figure 6) verify the presence of silica particles and CAP/Q co-precipitates. Furthermore, a variation between SAS1 and SAS2 processes was not observed, with stick-shaped particles obtained for both SAS1 and SAS2, usually identified as Q particles [30,31], NPs and MPs corresponding to CAP, and larger spheres corresponding to silica.

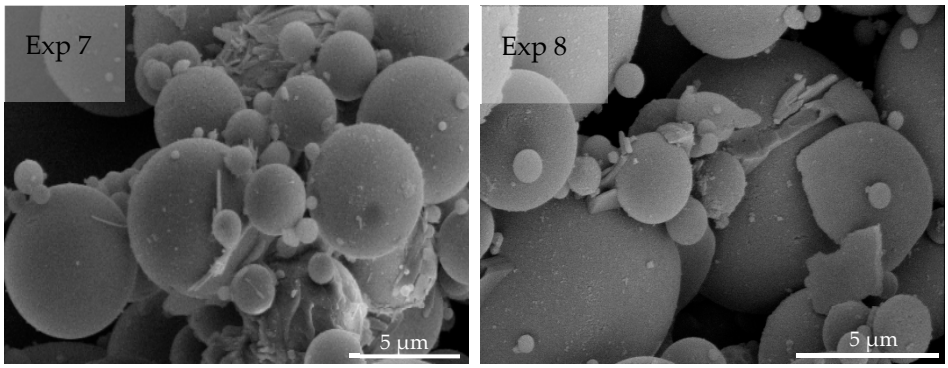

Figure 6. SEM images for deposition experiments 7 and 8.

In these experiments, the amount of co-precipitate with Q was lower than in experiments 5–6 with MNG, and this change was due to the experimental conditions used, which favored a higher precipitation of MNG than CAP, as described previously [31,34].

In order to confirm the presence of quercetin and mangiferin in the silica co-precipitates, 5 mg of each sample were dissolved in 50 mL of acetone/DMSO for MNG co-precipitates and 50 mL of ethanol for Q co-precipitates (Table 2). The contents in these solutions were measured by UV–VIS spectrophotometry at a wavelength of 365 nm using a previously obtained calibration curve.

Table 2. Quantity of antioxidant in 5 mg of sample.

Exp.	Quantity (mg)	Process	Co-Precipitate
5	1.58 ± 0.05	SAS2	CAP/MNG
6	2.36 ± 0.06	SAS1	CAP/MNG
7	0.302 ± 0.002	SAS1	CAP/Q
8	0.45 ± 0.01	SAS2	CAP/Q

It was observed that in experiments 7 and 8—corresponding to the use of quercetin—the concentration was significantly lower than in experiments 5 and 6, where the concentration of mangiferin was six times higher than quercetin for the SAS1 process and three times higher for the SAS2 process. The fact that the amount of MNG was higher than Q is not unexpected since the operating conditions imposed to achieve the "body-mass" are suitable for MNG according to previous studies carried out on CAP/MNG co-precipitation.

3.2. Release Test

The release experiments on both SGF and SIF were performed for experiment 6, which contained mangiferin co-precipitates and experiment 8, which contained quercetin co-precipitates. These two experiments were chosen because the products contained the highest amounts of antioxidant in the analyzed samples (Table 2). The release tests for the deposition of co-precipitates on silica particles were compared with release tests carried out on the antioxidant processed by SAS, co-precipitate CAP/Q and CAP/MNG in a 2:1 ratio and also with raw quercetin and mangiferin.

The release of composites with quercetin in both SGF and SIF is represented in Figures 7 and 8. It can be observed that in both diagrams the dissolution rate in the gastric fluid is lower than in the intestinal fluid for the deposition tests. This finding is due to the fact that quercetin is more soluble in the intestinal fluid [40]. It can be observed that the deposition of co-precipitate on silica using the SAS2 configuration increased the efficiency of the protection of the quercetin in SGF when compared to the co-precipitate with the same ratio but without silica [31], delaying the release during the first hour. However, it is very interesting to note that the deposition experiment showed a higher and burst release in the SIF when compared with the co-precipitation experiment without silica in the first 15 min. Finally, quercetin had a higher dissolution rate in all experiments, with the amount released reaching 100% in the first 15 min for processed Q and deposited composite, 30 min for the co-precipitate, and almost 4 h for raw Q. This demonstrates the effectiveness of the SAS method for micronizing and increasing the dissolution rate of this type of compound while providing protection for the active principle, in this case, the antioxidant in the gastric fluid.

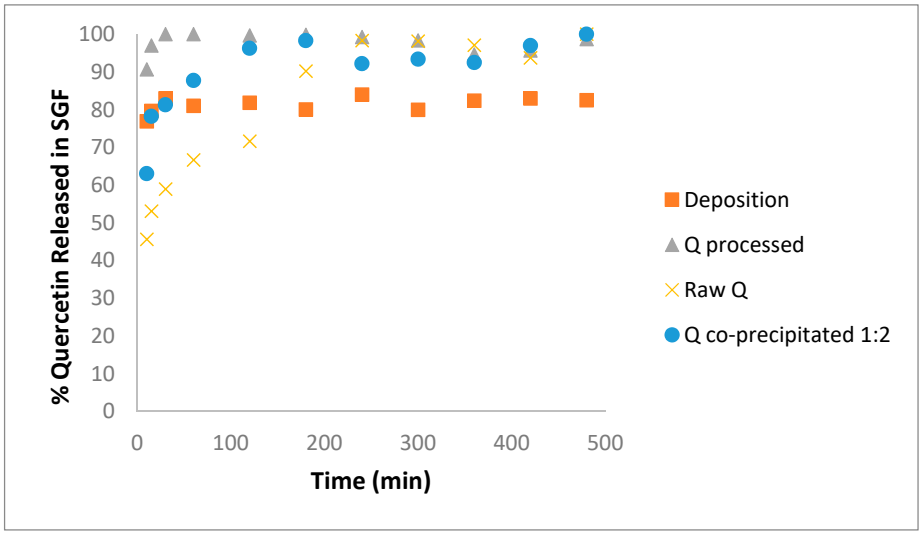

Figure 7. Release test of Q from composites in SGF corresponding to experiment 8 (180 bar, 323 K, 30 g/min CO_2 flow rate, SAS2).

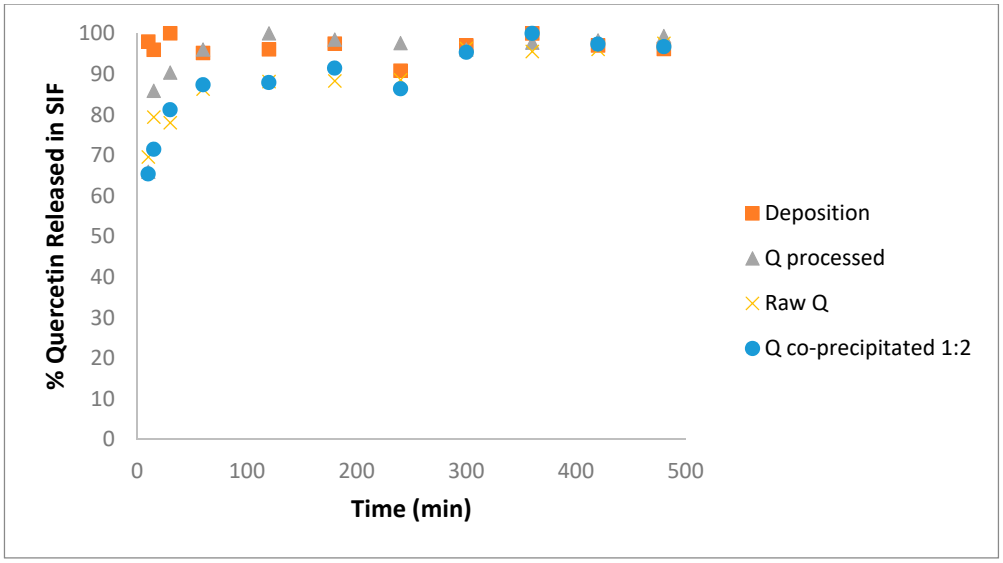

Figure 8. Release test of Q from composites in SIF corresponding to experiment 8 (180 bar, 323 K, 30 g/min CO_2 flow rate, SAS2).

In the case of mangiferin deposition, the same trend as for quercetin was found (Figures 9 and 10). A higher dissolution rate was observed in the intestinal fluid than in the gastric fluids. The protective effect of the polymer and silica with the MNG was evident. In SFG fluid, the antioxidant released after 8 h for the co-precipitate and deposited composites were around 50%, while the raw MNG was 80% and MNG processed by the SAS process was almost completely dissolved. In this case, the deposition experiment carried out in this work did not show any difference when compared with the co-precipitated experiment at the same ratio but without silica, which was carried out in a previous study [34] in SGF fluid. It can be observed, as in the case of Q, that in SIF the deposition experiment showed a burst release in the first 15 min—in contrast to the co-precipitation experiment. This fact could be associated with higher efficiency of the controlled release of the antioxidant in co-precipitate experiments in the absence of silica particles.

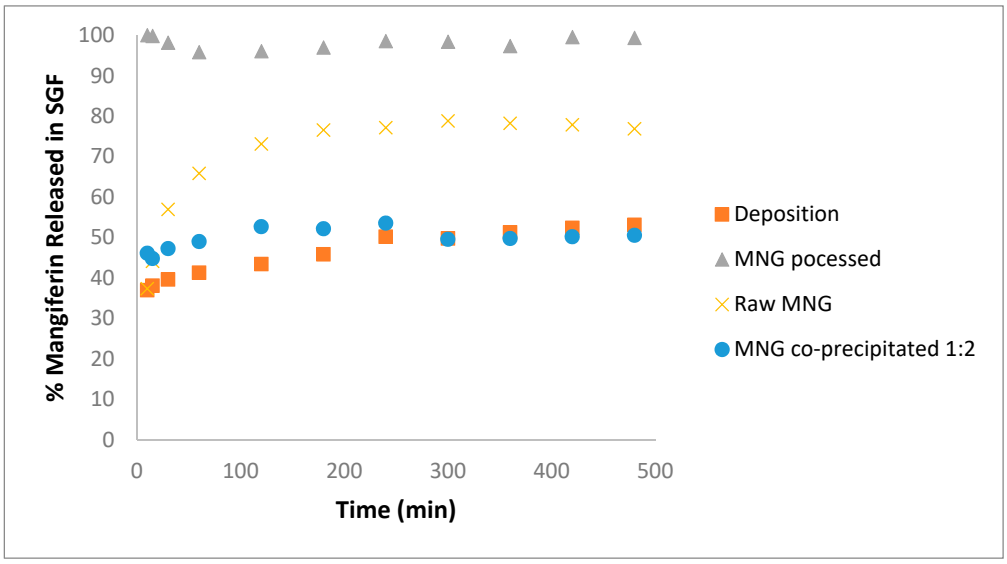

Figure 9. Release test of MNG from composites in SGF corresponding to experiment 6 (180 bar, 323 K, 30 g/min CO_2 flow rate, SAS1).

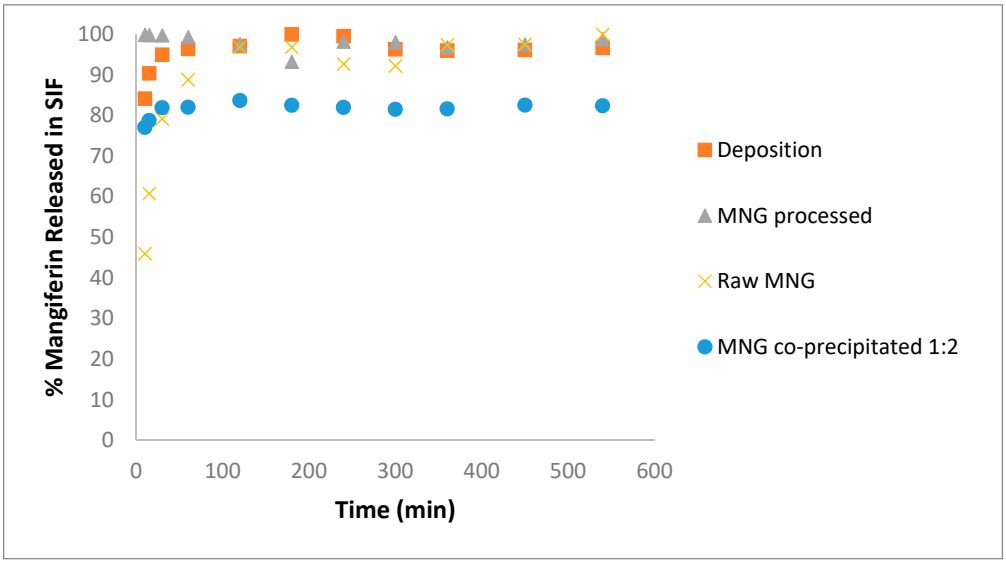

Figure 10. Release test of MNG from composites in SIF corresponding to experiment 6 (180 bar, 323 K, 30 g/min CO_2 flow rate, SAS1).

If the target is protecting the MNG in the gastric fluids due to its beneficial properties, this must be released and absorbed in the intestinal fluids. The experiments were successful because, in the SIF, the deposition experiment carried out with the SAS1 configuration made it possible to create composites of many compounds with a result as good as with the co-precipitate, i.e., increasing the solubility to almost 100% in the SIF. Finally, SAS1 and SAS2 gave similar results, although the versatility offered by the SAS2 configuration is advantageous in the use of different co-solvents for the polymer and the active principle.

4. Conclusions

Pressure and temperature conditions affect the success of the deposition process of the co-precipitates. The use of conditions well above the critical point of the mixture favors the deposition of the precipitates on silica. The low CO_2/dissolution flow rate ratio leads to precipitates with solvent residues and in less appreciable quantities. The deposition of the co-precipitates on the silica occurs mainly at the bottom of the precipitator under conditions far above of the MCP, with the presence of silica in the rest of the precipitator very limited. Both the SAS1 and SAS2 configurations are appropriate to deposit co-precipitates onto silica particles, with a slight difference observed in the morphology of the co-precipitate in the case of the MNG. The release of co-precipitate deposited on silica presents higher dissolution rates in SGF than in SIF for both antioxidants. The presence of silica inside the vessel during the SAS process provides mixed co-precipitate and matrix without an adverse effect on the benefits in terms of improving the protection of the active substance during the release test in SFG when compared to co-precipitate releases in the absence of silica. This approach also facilitated total and burst dissolution in SIF—in contrast to co-precipitate releases without the presence of silica.

Supplementary Materials: The following are available online at http://www.mdpi.com/2076-3417/10/13/4576/s1, Figure S1: Deposition images experiments 1,3-8.

Author Contributions: Conceptualization, A.M.; methodology, D.V.; formal analyses, E.J.M.d.l.O.; investigation, I.G.-C. and D.V.; writing—original draft preparation, A.M.; writing—review and editing A.M. and I.G.-C.; supervision, A.M. and C.P.; project administration, C.P.; funding acquisition, E.J.M.d.l.O. All authors have read and agreed to the published version of the manuscript.

Funding: This research was funded by the Spanish Ministry of Science and Technology (Project CTQ2017-86661-R). The APC was funded by the Spanish Ministry of Science and Technology (Project CTQ2017-86661-R).

Acknowledgments: We gratefully acknowledge the Spanish Ministry of Science and Technology (Project CTQ2017-86661-R) for financial support, and Central Service of Science and Technology of the University of Cádiz for analyses.

Conflicts of Interest: The authors declare no conflict of interest.

References

1. Jung, J.; Perrut, M. Particle design using supercritical fluids: Literature and patent survey. *J. Supercrit. Fluids* **2001**, *20*, 179–219. [CrossRef]
2. Martín, A.; Cocero, M.J. Micronization processes with supercritical fluids: Fundamentals and mechanisms. *Adv. Drug Deliv. Rev.* **2008**, *60*, 339–360. [CrossRef] [PubMed]
3. Reverchon, E.; De Marco, I. Supercritical fluid extraction and fractionation of natural matter. *J. Supercrit. Fluids* **2006**, *38*, 146–166. [CrossRef]
4. Essien, S.O.; Young, B.; Baroutian, S. Recent advances in subcritical water and supercritical carbon dioxide extraction of bioactive compounds from plant materials. *Trends Food Sci. Technol.* **2020**, *97*, 156–169. [CrossRef]
5. Matos, R.L.; Vieira de Melo, S.A.B.; Cabral Albuquerque, E.C.M.; Foster, N.R. Dense CO_2 technology: Overview of recent applications for drug processing/formulation/delivery. *Chem. Eng. Process. Process Intensif.* **2019**, *140*, 64–77. [CrossRef]
6. Reverchon, E. Supercritical antisolvent precipitation of micro- and nano-particles. *J. Supercrit. Fluids* **1999**, *15*, 1–21. [CrossRef]
7. Cocero, M.J.; Martín, Á.; Mattea, F.; Varona, S.; Martín, A.; Mattea, F.; Varona, S. Encapsulation and co-precipitation processes with supercritical fluids: Fundamentals and applications. *J. Supercrit. Fluids* **2009**, *47*, 546–555. [CrossRef]
8. Montes, A.; Baldauf, E.; Gordillo, M.D.; Pereyra, C.M.; Martínez de la Ossa, E.J. Polymer encapsulation of amoxicillin microparticles by SAS process. *J. Microencapsul.* **2014**, *31*, 16–22. [CrossRef]
9. Dias, A.M.A.; Braga, M.E.M.; Seabra, I.J.; de Sousa, H.C. Supercritical solvent impregnation of natural bioactive compounds in N-carboxybutylchitosan and agarose membranes for the devleopment of topical wound healing applications. *Lect. Notes Comput. Vis. Biomech.* **2012**, *1*, 243–266.
10. Guan, Y.; Yu, J.; Yao, S.; Zhu, Z. Preparation of control-released drugs using supercritical solution impregnation process. *Huagong Xuebao/CIESC J.* **2010**, *61*, 269–274.
11. Padrela, L.; Rodrigues, M.A.; Duarte, A.; Dias, A.M.A.; Braga, M.E.M.; de Sousa, H.C. Supercritical carbon dioxide-based technologies for the production of drug nanoparticles/nanocrystals—A comprehensive review. *Adv. Drug Deliv. Rev.* **2018**, *131*, 22–78. [CrossRef] [PubMed]
12. Girotra, P.; Singh, S.K.; Nagpal, K. Supercritical fluid technology: A promising approach in pharmaceutical research. *Pharm. Dev. Technol.* **2013**, *18*, 22–38. [CrossRef] [PubMed]
13. Available online: https://www.miyoshikaseigroup.com/en/surfacetreatment/surfacetreatment-type/silicone-type-treatment/sa-treatment/ (accessed on 25 July 2017).
14. Zhao, J.; Zhang, L.; Li, X.; Tao, X.; Zhu, W.; Ye, X. Supercritical CO_2 assisted fabrication of activated carbon-sulfur composite for improved lithium-sulfur batteries. *J. Alloys Compd.* **2017**, *708*, 264–269. [CrossRef]
15. Yen, C.H.; Lin, H.W.; Phan, T.D.; Tan, C.S. Chemical fluid deposition of monometallic and bimetallic nanoparticles on ordered mesoporous silica as hydrogenation catalysts. *J. Nanosci. Nanotechnol.* **2011**, *11*, 2465–2469. [CrossRef] [PubMed]
16. Aspromonte, S.G.; Sastre, Á.; Boix, A.V.; Cocero, M.J.; Alonso, E. Cobalt oxide nanoparticles on mesoporous MCM-41 and Al-MCM-41 by supercritical CO_2 deposition. *Microporous Mesoporous Mater.* **2012**, *148*, 53–61. [CrossRef]
17. Morère, J.; Tenorio, M.J.; Torralvo, M.J.; Pando, C.; Renuncio, J.A.R.; Cabañas, A. Deposition of Pd into mesoporous silica SBA-15 using supercritical carbon dioxide. *J. Supercrit. Fluids* **2011**, *56*, 213–222. [CrossRef]
18. Morère, J.; Torralvo, M.J.; Pando, C.; Renuncio, J.A.R.; Cabañas, A. Supercritical fluid deposition of Ru nanoparticles onto SiO_2 SBA-15 as a sustainable method to prepare selective hydrogenation catalysts. *RSC Adv.* **2015**, *5*, 38880–38891. [CrossRef]
19. Boots, A.W.; Haenen, G.R.M.M.; Bast, A. Health Effects of Quercetin: From Antioxidant to Nutraceutical. *Eur. J. Pharmacol.* **2008**, *585*, 325–337. [CrossRef]
20. Sahoo, N.G.; Kakran, M.; Shaal, L.A.; Li, L.; Müller, R.H.; Pal, M.; Tan, L.P. Preparation and characterization of quercetin nanocrystals. *J. Pharm. Sci.* **2011**, *100*, 2379–2390. [CrossRef]

21. Rajendran, P.; Rengarajan, T.; Nandakumar, N.; Divya, H.; Nishigaki, I. Mangiferin in cancer chemoprevention and treatment: Pharmacokinetics and molecular targets. *J. Recept. Signal Transduct.* **2015**, *35*, 76–84. [CrossRef] [PubMed]
22. Carvalho, R.; Pellizzon, C.H.; Justulin, L., Jr.; Felisbino, S.L.; Vilegas, W.; Bruni, F.; Lopes-Ferreira, M.; Hiruma-Lima, C.A. Effect of mangiferin on the development of periodontal disease: Involvement of lipoxin A4, anti-chemotaxic action in leukocyte rolling. *Chem. Biol. Interact.* **2009**, *179*, 344–350. [CrossRef]
23. Van der Merwe, J.D.; Joubert, E.; Manley, M.; de Beer, D.; Malherbe, C.J.; Gelderblom, W.C.A. Mangiferin glucuronidation: Important hepatic modulation of antioxidant activity. *Food Chem. Toxicol.* **2012**, *50*, 808–815. [CrossRef] [PubMed]
24. Srinivas, K.; King, J.W.; Howard, L.R.; Monrad, J.K. Solubility and solution thermodynamic properties of quercetin and quercetin dihydrate in subcritical water. *J. Food Eng.* **2010**, *100*, 208–218. [CrossRef]
25. Liu, M.; Liu, Y.; Ge, Y.; Zhong, Z.; Wang, Z.; Wu, T.; Zhao, X.; Zu, Y. Solubility, antioxidation, and oral bioavailability improvement of mangiferin microparticles prepared using the supercritical antisolvent method. *Pharmaceutics* **2020**, *12*, 90. [CrossRef]
26. Montes, A.; Wehner, L.; Pereyra, C.; Martínez de la Ossa, E.J. Mangiferin nanoparticles precipitation by supercritical antisolvent process. *J. Supercrit. Fluids* **2016**, *112*, 44–50. [CrossRef]
27. Liu, X.; Li, Z.; Han, B.; Yuan, T. Supercritical antisolvent precipitation of microparticles of quercetin. *Chin. J. Chem. Eng.* **2005**, *13*, 128–130.
28. Santos, D.T.; Meireles, M.A.A. Micronization and encapsulation of functional pigments using supercritical carbon dioxide. *J. Food Process Eng.* **2013**, *36*, 36–49. [CrossRef]
29. Fernández-Ponce, M.T.; Masmoudi, Y.; Djerafi, R.; Casas, L.; Mantell, C.; de La Ossa, E.M.; Badens, E. Particle design applied to quercetin using supercritical anti-solvent techniques. *J. Supercrit. Fluids* **2015**, *105*, 119–127. [CrossRef]
30. Montes, A.; Pereyra, C.; Martínez de la Ossa, E.J. Screening design of experiment applied to the supercritical antisolvent precipitation of quercetin. *J. Supercrit. Fluids* **2015**, *104*, 10–18. [CrossRef]
31. García-Casas, I.; Montes, A.; Pereyra, C.; Martínez de la Ossa, E.J. Generation of quercetin/cellulose acetate phthalate systems for delivery by supercritical antisolvent process. *Eur. J. Pharm. Sci.* **2017**, *100*, 79–86. [CrossRef]
32. Garg, A.; Rai, G.; Lodhi, S.; Jain, A.P.; Yadav, A.K. Hyaluronic acid embedded cellulose acetate phthlate core/shell nanoparticulate carrier of 5-fluorouracil. *Int. J. Biol. Macromol.* **2016**, *87*, 449–459. [CrossRef] [PubMed]
33. E Silva, J.P.S.; Sousa, S.C.; Costa, P.; Cerdeira, E.; Amaral, M.H.; Lobo, J.S.; Gomes, A.M.; Pintado, M.M.; Rodrigues, D.; Rocha-Santos, T.; et al. Development of probiotic tablets using microparticles: Viability studies and stability studies. *AAPS PharmSciTech* **2013**, *14*, 121–127. [CrossRef] [PubMed]
34. García-Casas, I.; Montes, A.; Pereyra, C.; Martínez de la Ossa, E.J. Co-precipitation of mangiferin with cellulose acetate phthalate by Supercritical antisolvent process. *J. CO2 Util.* **2017**, *22*, 197–207. [CrossRef]
35. Reverchon, E.; Caputo, G.; De Marco, I. Role of Phase Behavior and Atomization in the Supercritical Antisolvent Precipitation. *Ind. Eng. Chem. Res.* **2003**, *42*, 6406–6414. [CrossRef]
36. Denardin, F.G.; Vieira De Melo, S.A.B.; Mammucari, R.; Foster, N.R. Phase transition and volume expansion in CO_2-expanded liquid systems. *Chem. Eng.* **2013**, *32*, 529–534.
37. Joung, S.N.; Yoo, C.W.; Shin, H.Y.; Kim, S.Y.; Yoo, K.-P.; Lee, C.S.; Huh, W.S. Measurements and correlation of high-pressure VLE of binary CO_2–alcohol systems (methanol, ethanol, 2-methoxyethanol and 2-ethoxyethanol). *Fluid Phase Equilib.* **2001**, *185*, 219–230. [CrossRef]
38. Zhu, Y.F.; Shi, J.L.; Li, Y.S.; Chen, H.R.; Shen, W.H.; Dong, X.P. Storage and release of ibuprofen drug molecules in hollow mesoporous silica spheres with modified pore surface. *Microporous Mesoporous Mater.* **2005**, *85*, 75–81. [CrossRef]
39. Martín, A.; Cocero, M.J. Numerical modeling of jet hydrodynamics, mass transfer, and crystallization kinetics in the supercritical antisolvent (SAS) process. *J. Supercrit. Fluids* **2004**, *32*, 203–219. [CrossRef]
40. Fraile, M.; Buratto, R.; Gómez, B.; Martín, Á.; Cocero, M.J. Enhanced delivery of quercetin by encapsulation in poloxamers by supercritical antisolvent process. *Ind. Eng. Chem. Res.* **2014**, *53*, 4318–4327. [CrossRef]